Jour. Fac. Sci., Hokkaido Univ., Ser. VII (Geophysics), Vol. 11, No. 6, 821-844, 2002.

Development Processes of Convective Cloud System during the Approach of the Meiyu Front in the Latter Half of GAME/HUBEX IOP 1998

Mayumi Yoshida* and Hiroshi Uyeda**

Division of Earth and Planetary Sciences, Graduate School of Science, Hokkaido University, Sapporo 060-0810, Japan

(Received December 15, 2001)

Abstract

We made radar observations during GAME/HUBEX IOP 1998 from June to July and analyzed development processes of convective cloud systems observed in the radar site which located in the south of the formation and approach of the Meiyu front from 10 to 16 July.

The features and structures of the observed convective cloud systems changed in relation to the approach of the Meiyu front with the increase of water vapor and modification of vertical wind shear. The echo top height was influenced by the water vapor in the middle or upper layer while the direction of new echo generation depended on the vertical wind shear. Strong advection with the southerly component along and toward the Meiyu front was significant to determine the features of the convective cloud systems in the southern region of the Meiyu front.

We also suggest the possibility that the convective cloud clusters played an important role in transporting water vapor to the Meiyu front in the process of their formation.

1. Introduction

The Meiyu front in China and the Baiu front in Japan are one of the most significant circulation systems for energy and water cycle in the East Asian monsoon region.

There have been many studies about moisture transport to the Meiyu and the Baiu front. Murakami (1959) stated that there existed four kinds of prevailing wind systems which were called in his paper as Polar jet, Indian westerlies,

* Present affiliation: Remote Sensing Technology Center of Japan, Tokyo 104-6021, Japan

** Present affiliation: Hydrospheric Atmospheric Research Center, Nagoya University, Nagoya 464-8601, Japan

Baiu jet and Easterlies respectively. He continued that in early stage of the season, moisture flow accomplished by Indian westerlies played an important role for shaping the distributions of rainfall in the fronts, however in the last stage moisture flow from the southern Pacific became significant. Moreover he pointed out the importance of evaporation to the east of Formosa. As the origin of moisture, Saito (1966) indicated that the China continent were also important.

Smaller scale studies about the Baiu front have also been made. The Baiu front was characterized as a large gradient of atmospheric water vapor (Matsumoto et al., 1970). Akiyama (1973a) pointed out the close relation between a low-level jet stream and areas of heavy rainfall. Using moisture budget analysis, Matsumoto et al. (1971) and Akiyama (1975) showed that the vast amounts of water vapor were transported to the Baiu frontal zone by the low-level southerly and southwesterly flows. Ninomiya and Akiyama (1992) reviewed the recent studies, and concluded that motions of many scales were interacting with each other, which was the most outstanding feature of the Baiu.

However, there are less mesoscale studies about the Meiyu front in China. Chen et al. (1998) simulated heavy rainfall events using a mesoscale model and suggested that there was strong interaction and positive feedback between the convective rainstorms embedded within the Meiyu front and the Meiyu front itself. The front provided a favorable environment for such rainstorms to develop, and the rainstorms intensified the Meiyu front.

To confirm such a model study, more detail observations about the Meiyu front were necessary. For that reason, HUaihe river Basin EXperiment (HUBEX) was implemented (Zhao and Takeda, 1998) as taking charge of subtropical and temperate monsoon regions of East Asia in GEWEX Asian Monsoon Experiment (GAME). This area is characterized largely by the Meiyu front in summer. In the Meiyu front, various scales of cloud systems are formed and play an important role in the energy and water cycle.

In HUBEX IOP (Intensive Observation Period), we observed the cloud systems that developed to the south of the Meiyu front in addition to that on the front. But the studies about convective cloud to the south of the Meiyu front are a little. Kato et al. (1995) examined the appearance frequency of Cb-clusters and its diurnal variation in relation to large scale conditions, and showed that in the area covered by the subtropical high, the isolated Cb-clusters developed very frequently in the evening in spite of the strong low-level divergence. Nakai and Kawamura (1998) investigated the appearance frequency of 74 of mesoscale cloud clusters by using GMS/IR data and showed that most of

the meso-α scale cloud clusters tended to appear in the vicinity of the Baiu front with their lifetime being more than 13 hours while many of meso-β scale cloud clusters were in the subtropical high with short lifetime less than 12 hours. As these cases, the diurnal variation of smaller scale cloud clusters were observed also under the subtropical high.

The south of the Meiyu frontal zone is the area of moisture transport and the convection by the cloud lead to the vertical moisture transport. Therefore, to clarify the convective cloud system in the south area is supposed to be important in understanding moisture transport to the Meiyu frontal zone.

The purpose of this study is to investigate development process of convective cloud systems to the south of the Meiyu front in the process of the formation and approach of the front using the data obtained in HUBEX IOP in 1998.

2. Observations and analytical method

2.1 Observations

During the GAME/HUBEX IOP (from June 11 to July 17) in 1998, Doppler radar and Radiosonde observations were carried out in Anhui Province, China. At the end of the IOP, from July 10 to July 15, diurnal variations of cloud cluster were observed. Three Doppler radar sets, which detection range was 60 km in radius, were positioned at Huainan (Hokkaidou University Doppler radar), Shuxian and Fengtai (Nagoya University Doppler radar) as shown in Fig. 1. Their volume scan data were basically acquired at the same time at 7 minutes intervals for dual-Doppler analysis.

During the IOP, sounding station network (AREA1 in Fig. 1), each taking high-resolution soundings 4 times per day, was set up around the radar observation ranges. Hourly infrared (IR) data from the GMS-5 (Geostational Meteorological Satellite) was also utilized.

2.2 Analytical method

We used dual-Doppler radar data to calculate three-dimensional wind fields. The Cressman's method (Cressman, 1959) with influence radii of 1.0 km was employed to interpolate the raw data in the polar coordinate to the Cartesian coordinate. The grid interval was 1 km in horizontal and 0.25 km in vertical. Using the rearranged Doppler velocity and a mass continuity equation, vertical wind-velocities were derived from upward integration of horizontal divergence from lower boundary where vertical velocity supposed to be zero.

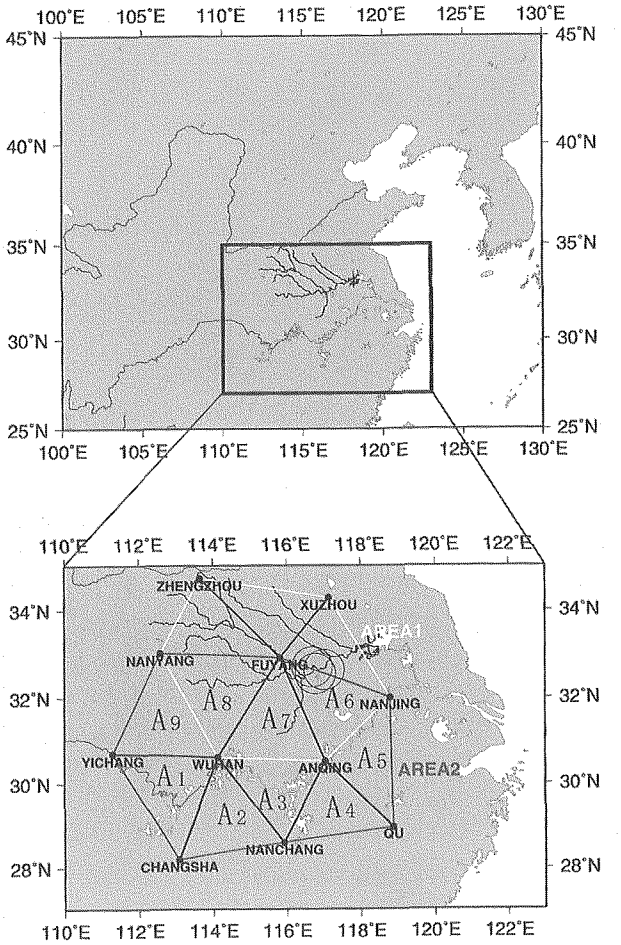

Fig. 1. Radar observation and analysis region. Three Doppler radar observation ranges and sounding sites are shown by circles and dots respectively. AREA1 shown by white hexagon indicate the high-resolution sounding station network and AREA2 shown by gray polygon is the area where we made the water budget analysis.

Then they were corrected assuming zero at the higher boundary. In case of this analysis, it was necessary to take system movement into account. So we adopted Gal-Chen's method (Gal-Chen, 1982) for the correction.

We also analyzed water vapor budget for the purpose of understanding moisture transport. Following Yanai et al. (1973), the apparent moisture sink Q_2 are expressed as

$$Q_2 \equiv -L\left(\frac{\overline{\partial q}}{\partial t}+\overline{\nabla \cdot qV}+\frac{\overline{\partial \omega}}{\partial p}\right),$$

where q is the specific humidity, L is the latent heat of condensation, V is the horizontal wind vector and ω is the vertical wind velocity in pressure (p) coordinates. Over-bars represent the horizontal averages in the domain of interest.

Actually, to calculate each term using the available sounding data, the following methods were employed. Mean vertical p-velocity was obtained from mass continuity equation by integrating mean horizontal wind divergences that were calculated at the triangle area consisting of each sounding site assuming $\overline{\omega}=0$ ($Pa \cdot s^{-1}$) at the surface. However, $\overline{\omega}$ became less accurate as height increase, so we made correction based on the assumptions that mean vertical p-velocity was zero at 200 hPa. Also, time derivative of averaged specific humidity was calculated from values at ± 6 h of a given time.

3. Results

3.1 Environmental conditions

The location of the front around the radar site from 12 July to 18 July is shown in Fig. 2. The Meiyu front extended around the Yellow River on 10 July then moved eastward, while the Huaihe River Basin was covered with the subtropical high. However, a polar front generated to the north of 40°N on 12

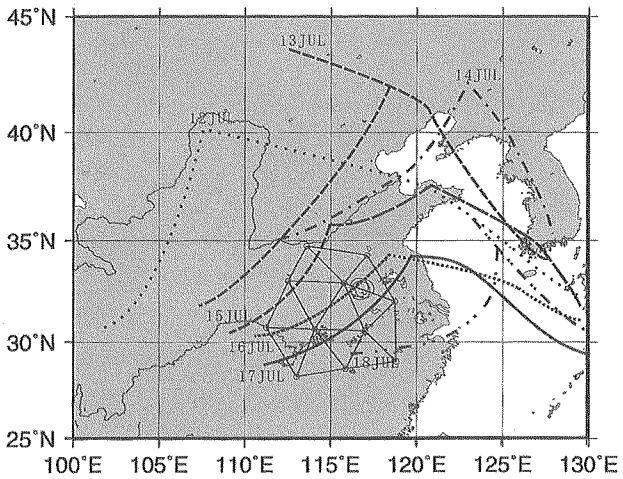

Fig. 2. Fronts around the radar sites from 12 July to 18 July 1998.

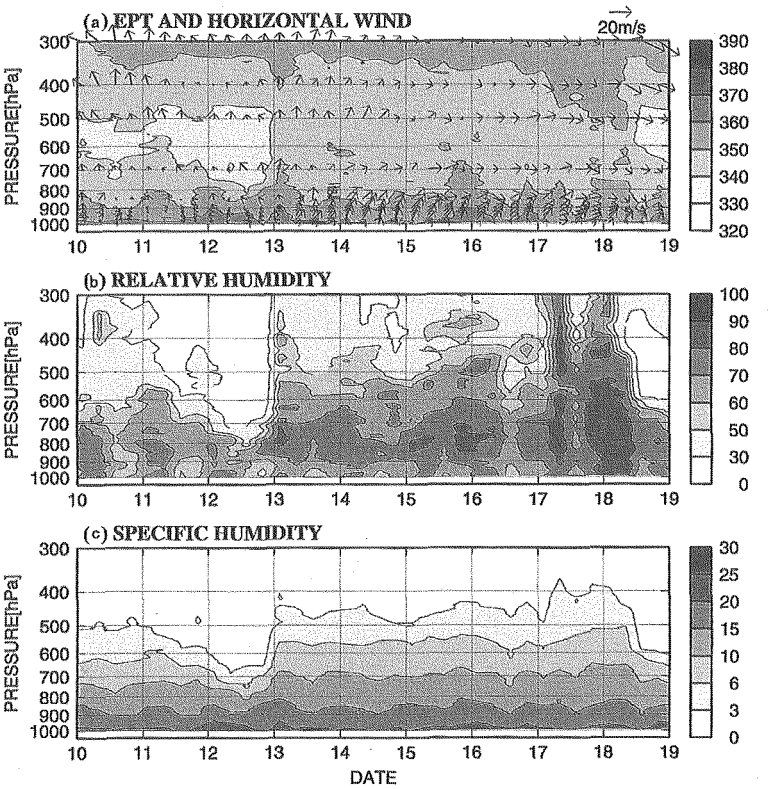

Fig. 3. Time variations of environmental conditions at Anqing from 10 July to 18 July 1998. (a) Equivalent potential temperature and horizontal wind, (b) relative humidity, and (c) specific humidity.

July moved eastward and formed a Meiyu front on 14 July. Then it moved southward and passed around the radar site from 16 July to 17 July.

To examine the changes of environmental conditions in the process of front going south, time series of equivalent potential temperature, relative humidity, specific humidity and horizontal wind at Anqing, which is sounding site windward of the radar site, are shown in Fig. 3. We see strong convectively unstable layer below 600 hPa from 10 July to 13 July, getting less unstable after that. Then almost neutral condition was observed at Fuyang the nearest sounding site on 17 July when the Meiyu front existed around radar site (not shown). This means that the further the site was southward from the Meiyu front, the more convectively unstable it became, and agreed with the result obtained in Akiyama (1973b).

Also, both relative humidity and specific humidity suddenly increased especially above 700 hPa between 20 BST 12 July and 02 BST 13 July at Anqing, and 08 BST and 14 BST on July 13 at Fuyang. Therefore it seems that water vapor increased from around 02 BST to 08 BST on 13 July in the vicinity of the radar site.

We can see the change of horizontal wind in connection with the front movement. On 10 July and 11 July, the wind speed at low level was weak with weak vertical shear as the site was under the subtropical high. It appeared southeasterly wind, which blew into a low-pressure system, especially in the lower layer on 12 July. Then as the low moved east and a cold front approached to the site on 13 July, the wind at low level turned into relatively weak southwesterly one and the strong southerly wind along the front was observed at middle and upper level. When the front moved south further (after 14 July), strong southwesterly winds flowing into the Meiyu front were seen at the lower altitude. And after the passage of the front from 16 July to 17 July, the wind direction changed northerly.

3.2 Development processes of convective cloud system

In this subsection, we describe the features and structures of the convective cloud system observed in the radar site accompanied by the changes of the environmental conditions presented in the previous subsection.

Figure 4 shows time series of the echo top height, echo area at 2 km height and the GMS-IR area under each brightness temperature observed in the radar site from 10 July to 18 July, but the echo on 12 July was not precipitation one. We see from the figure the diurnal variation that convective precipitation fell during afternoon in the period from 10 July to 15 July. It was likely because sensible heat flux from the ground produced the most unstable conditions during the afternoon. In contrast not a diurnal convective system in the Meiyu frontal zone was observed between 19 BST on 16 July and in the morning on 17 July. Moreover the features changed suddenly on 13 July that is to say echo top height had reached 16 km since 13 July while about 8 km on 10 July and 11 July, and GMS-IR area increased. The intensification of the convective activity followed water vapor increase as mentioned above.

Next, we make a comparison of four cases on 11, 13, 14 and 16 July in terms of the structure of convective systems. The cloud system was maintained in the radar site for about three hours on 11 July, about six hours on 13 July, about seven hours on 14 July and more than 10 hours on 16 July with successively producing new cells. To understand how the systems developed and

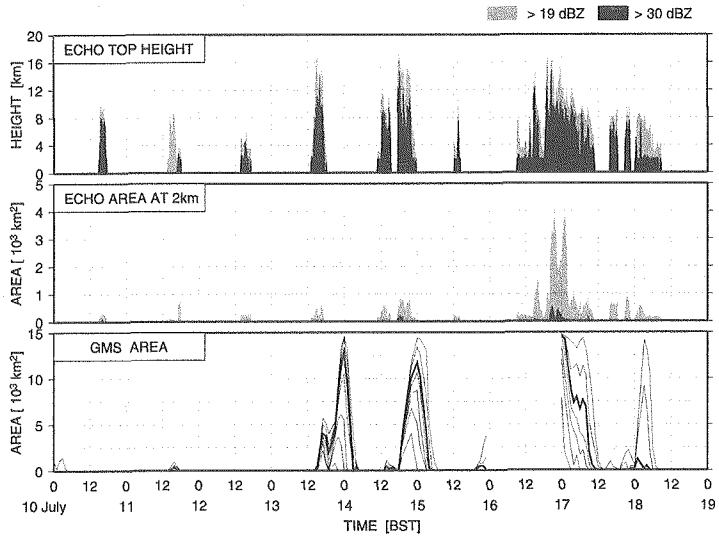

Fig. 4. Time series of echo top height and echo area at 2 km (gray shade>19 dBZ and dark shade>30 dBZ) of Huainan radar from 10 July to 18 July 1998. Cloud area of TBB of GMS-5/IR in the area of 121 km×121 km over Huainan Doppler radar observation range is shown in the bottom. Contours are from 0°C every 10°C. Thick contour indicates 20°C.

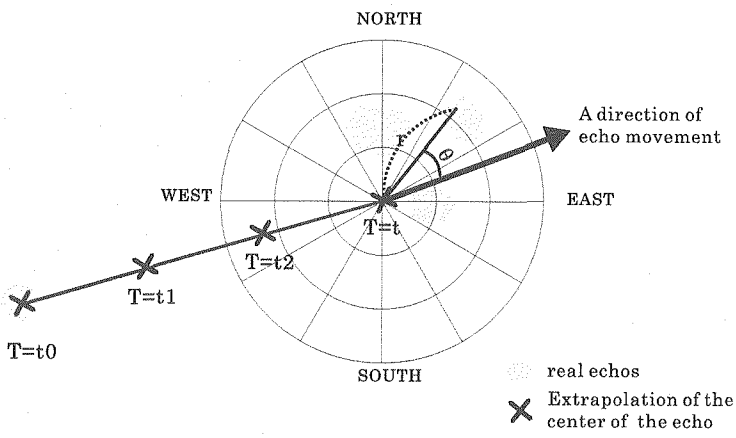

Fig. 5. The method to analyze the trend of new cell generation.

maintained, we analyzed where the new cells tended to be generated relative to the existing ones in the way explained in Fig. 5. First we got the velocity of the cell movement at an initial time ($T=t_0$), second decided the location of the cell supposed to be at each time ($T=t$) by extrapolating the initial velocity, and

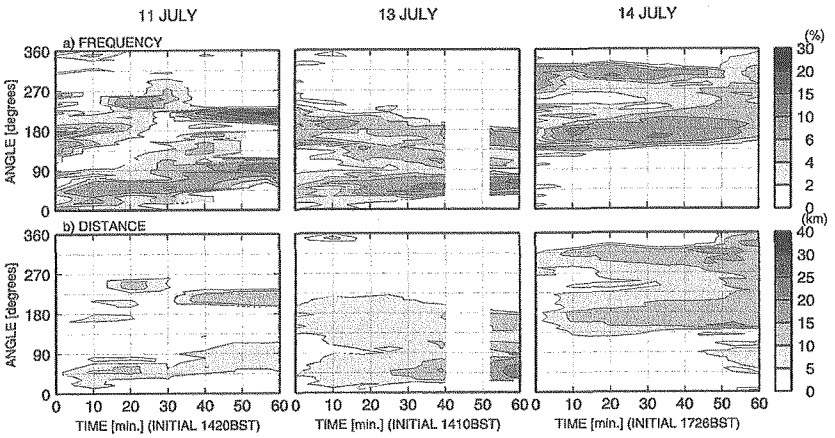

Fig. 6. Time series of (a) the frequency and (b) the mean distance of the real echoes at the angle every 10 degrees counterclockwise from a direction of echo movement on 11, 13, 14 July 1998. The initial time (t_0 in Fig. 5) for 11, 13 and 14 July are 1420 BST, 1410 BST and 1726 BST respectively.

third calculated the frequency and mean distance (r) of the echoes existing actually to the location at each ten degrees (θ). The results of the analysis on 11, 13, 14 July are depicted in Fig. 6, but the analysis could not be conducted on 16 July because line-oriented precipitation systems came into the site so the initial echo was not identified. The direction having tendency of producing new cell can be read from the figure. On 11 July, the formation of new cells occurred at all directions. On the other hand, the frequency (Fig. 6a) was concentrated from 45 to 90 degrees and 180 degrees on 13 July. While the mean distance at 180 degrees was almost constant, it increased gradually between 45 to 90 degrees. It means that at first a new cell was generated both on the north and the southwest sides, then on the north side a newer cell was successively produced on the further north side; to put it simply, new cell was apt to be generated on the north side on 13 July. On 14 July, we see that new cell tended to produce on the southerly part, especially on the southwest side.

As mentioned above, the location for new cell generation varied with the days. In order to clarify the cause, we examined the wind fields using dual-Doppler radar analyses.

a) 11 July

On 11 July, the vertical wind shear of the horizontal wind below 5 km height was weak as shown in the wind hodograph (Fig. 7) at 14 BST at Fuyang. Figure 8 shows Constant Altitude Plan Position Indicator (CAPPI) of radar

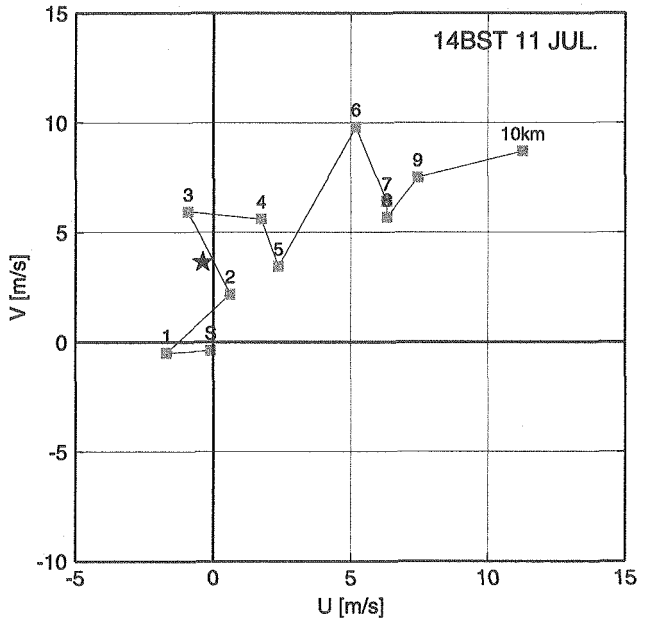

Fig. 7. Wind hodograph at Fuyang at 14 BST 11 July 1998. Echo movement is shown by a solid star.

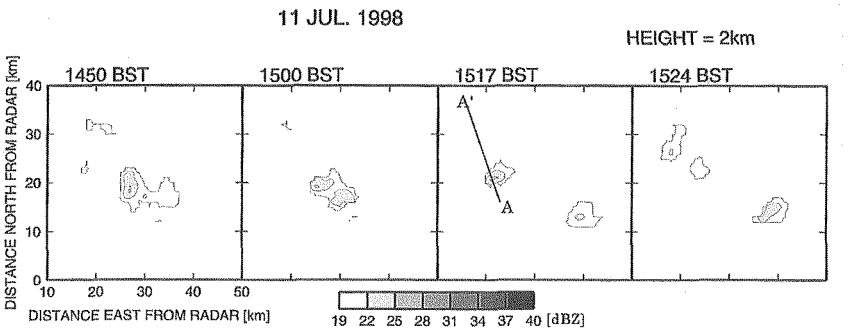

Fig. 8. CAPPI of the reflectivity at the level of 2 km observed by Huainan Doppler radar from 1450 BST to 1524 BST on 11 July 1998. Contours are every 3 dBZ from 19 dBZ.

reflectivity at a height of 2.0 km from 1450 BST to 1524 BST on 11 July. New echo was generated on both sides as mentioned above. As in the vertical cross section (Fig. 9) along the line A-A′ in Fig. 8, the echo top was relatively low and low-level outflows were seen on both sides of a downdraft.

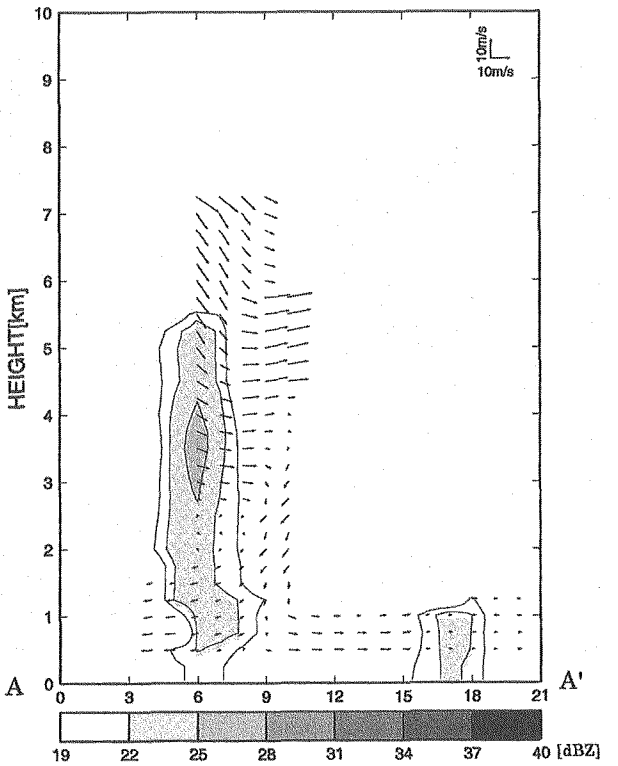

Fig. 9. Vertical cross section along the line A-A′ in Fig. 8 at 1517 BST 11 July 1998. Radar reflectivity is shown by the shade and contours every 3 dBZ from 19 dBZ. The vectors denote the ground relative winds by dual-Doppler radar analyses.

b) 13 July

On 13 July strong vertical wind shear of the horizontal wind between the surface to 5.2 km height can be seen from the wind hodograph at 14 BST (Fig. 10). Under this environment the convective system as shown in Fig. 11 was observed. Thought the new cell was produced at north (M) and southwest (N) sides of the initial one (L), southwest cell (N) dissipated gradually while north one developed with producing newer cell to the north. This agreed with the situation described in Fig. 6.

Figure 12 shows the vertical cross section of reflectivity and wind vector relative to echo movement along line the B-B′ in Fig. 11 at 1503 BST. In fourteen minutes after this, a new cell was generated to the north of the cell. It seems to be mature to dissipating stage because the reflectivity core reached to

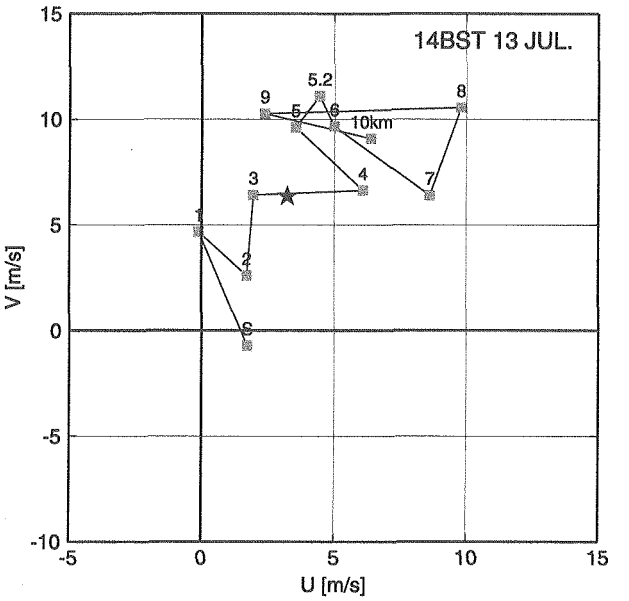

Fig. 10. Same as Fig. 7 except at 14 BST 13 July 1998.

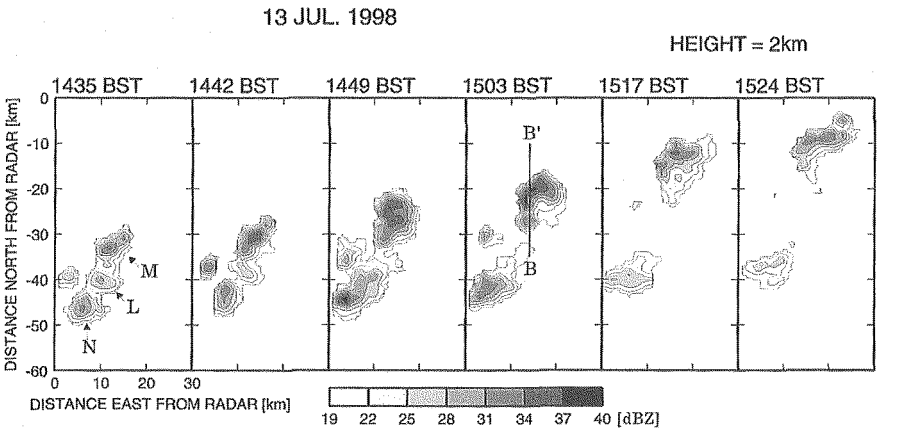

Fig. 11. Same as Fig. 8 except from 1435 BST to 1524 BST on 13 July 1998.

the ground and downdraft was seen in the lower layer. The low-level southerly outflow from the downdraft and the environmental northerly wind caused convergence on the north side of the older cell around 1 km height.

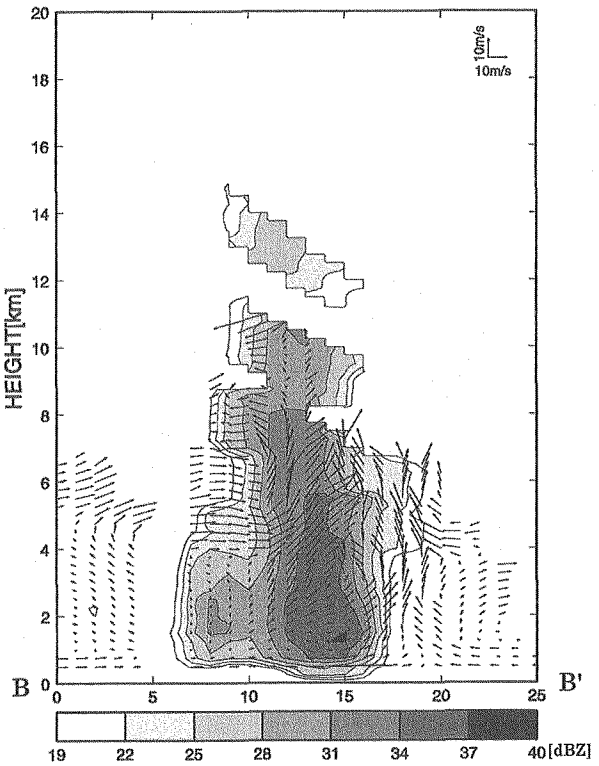

Fig. 12. Vertical cross section along the line B-B′ in Fig. 11 at 1503 BST 13 July 1998. Radar reflectivity is shown by the shade and contours every 3 dBZ from 19 dBZ. The vectors denote the winds relative to the echo movement by dual-Doppler radar analysis.

c) 14 July

It can be seen from the wind hodograph (Fig. 13) that southwesterly wind was dominant in the lower layer on 14 July. New cell was generated on the southwest side of the existing cell from CAPPI at 2.0 km height (Fig. 14). Figure 15 is the vertical cross section along the line C-C′ in Fig. 14. Though data is missing above 7 km height, downdraft existed at least below 6 km height and outflow flew to southwest. Moreover it converged with the environmental southwesterly wind on the southwest side.

d) 16 July

On 16 July, the squall line extended from the northwest to the southeast and moved northeastward at about 12 m/s as shown in Fig. 16. The convective cells were aligned at its leading edge and a stratiform region extended behind them

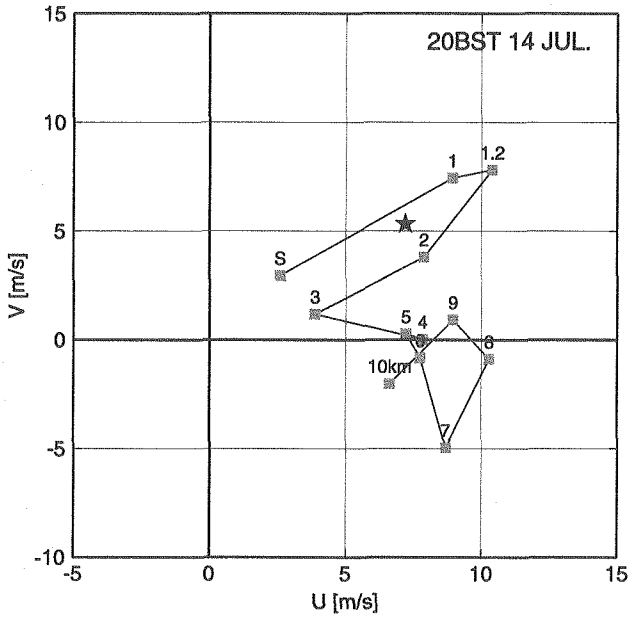

Fig. 13. Same as Fig. 7 except at 20 BST 14 July 1998.

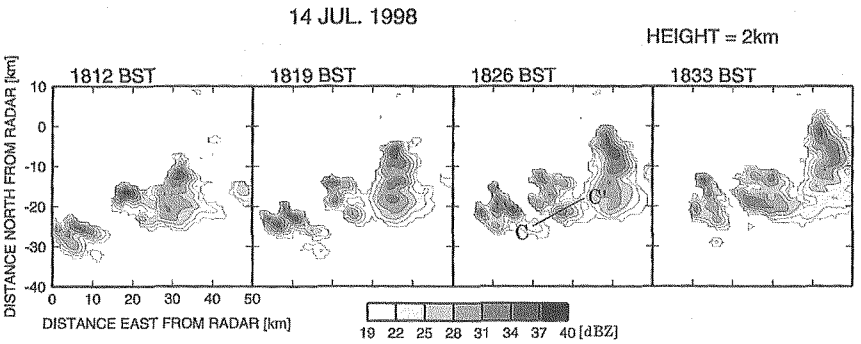

Fig. 14. Same as Fig. 8 except from 1812 BST to 1833 BST on 14 July 1998.

thought it is not clear due to the attenuation. The wind hodograph at 20 BST on 16 July is represented in Fig. 17; strong vertical wind shear parallel to the system movement existed from surface to 4 km height. This feature is similar to that of fast-moving tropical mesoscale convective cloud lines presented in Barnes and Sieckman (1984). Figure 18 shows the vertical cross section of reflectivity and the system relative wind vector along the line D-D′ at 1901 BST

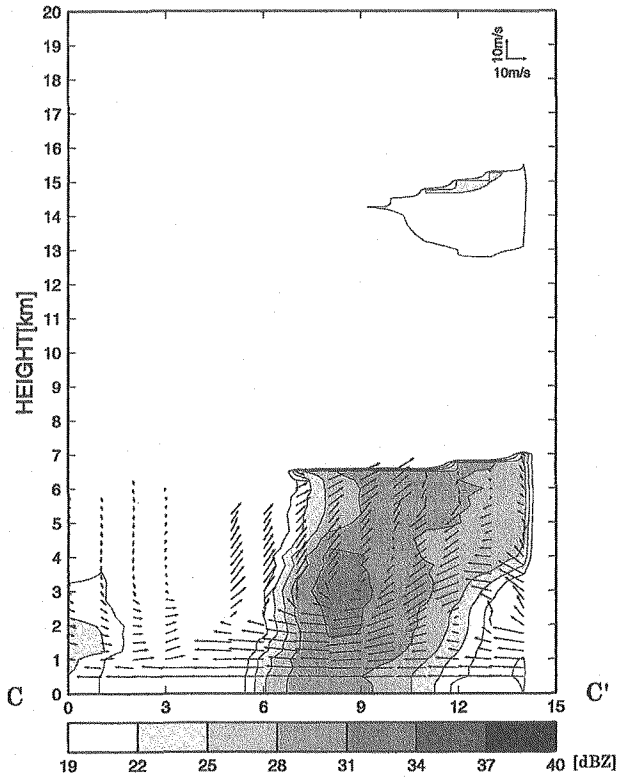

Fig. 15. Same as Fig. 12 except along the line C-C′ in Fig. 14 at 1826 BST 14 July 1998.

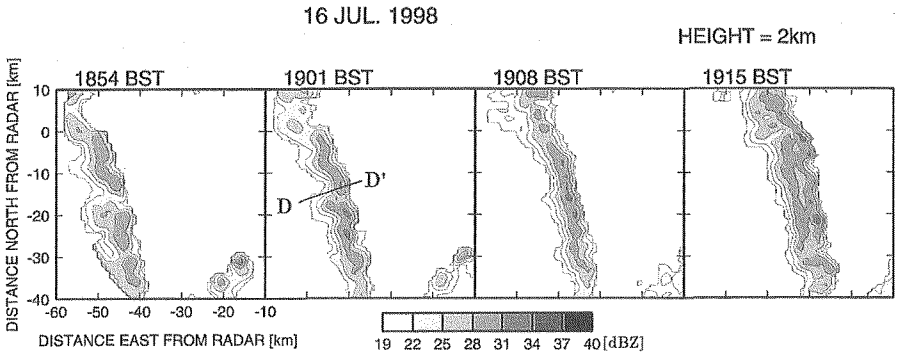

Fig. 16. Same as Fig. 8 except from 1854 BST to 1915 BST on 16 July 1998.

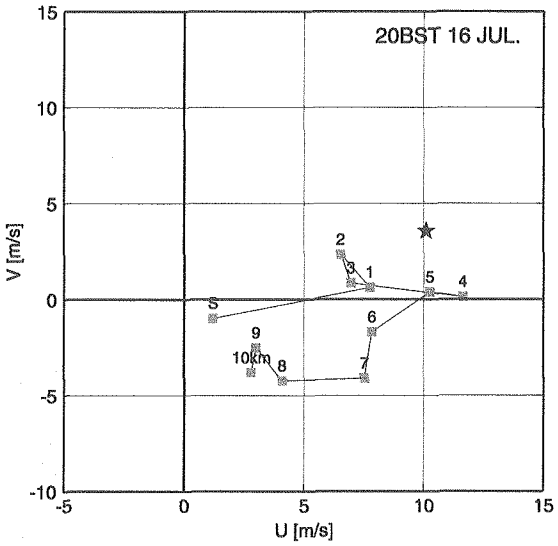

Fig. 17. Wind hodograph at Fuyang at 20 BST 16 July 1998. The system movement is shown by the star.

in Fig. 16. Above the height of 1 km, the wind flowing into the storm was observed ahead of the line. A well known front-to-rear flow at middle and upper level and rear-to-front flow under the level was also presented in this case.

3.3 Moisture transport

In this subsection, the source of the water vapor increase between 12 July and 13 July followed by the intensification of convective activity are explored.

a) Movement of cloud cluster

Figure 19 shows the GMS-IR imageries at every three hours from 08 BST 12 July to 11 BST 13 July, however the image at 01 BST 13 July is shown alternatively because we have no data at 02 BST 13 July. We can see the cloud clusters associated with tropical cyclone in the vicinity of Taiwan at 08 BST and 11 BST, which was also observed at night and during early morning on 10 July and 11 July. Then new mesoscale convective clouds were successively generated to the north of them after 14 BST which is the favorable time for convection over the continent. Consequently, the cloud clusters moved northward on the whole. After 23 BST, they seemed to be stratified gradually. The continuation is shown in Fig. 20, consisted of hourly imageries from 13 BST to 17 BST on 13 July. It can be seen from this figure that convective clouds was generated

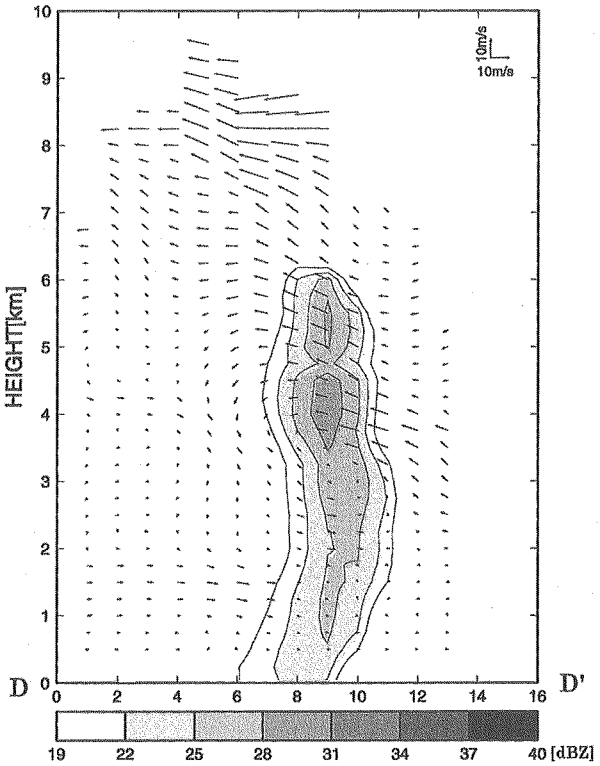

Fig. 18. Vertical cross section along the line D-D′ line in Fig. 16 at 1901 BST 16 July 1998. Radar reflectivity is shown by the shade and contours every 3 dBZ from 19 dBZ. The vectors denote the system relative winds by dual-Doppler radar analysis.

again at the tip and to the north of the region which used to be of the cloud clusters the day before, after 13 BST or 14 BST that is to say convective time. It was the part of this that we could observe in the radar site.

b) Apparent moisture source

As we have discussed about the movement of cloud clusters during afternoon, next we investigate what occurred at night or during early morning when the convective activity was suppressed. For this purpose, we made water vapor budget analysis over the AREA2 in Fig. 1.

The results at 02 BST on 13 July are shown in Fig. 21. A GMS IR image, one hour before that time, was denoted with an arrow in Fig. 19. As mentioned in the previous subsection, the cloud cluster was turning to stratiform and the tip was hanging over southwesterly part of the analysis area. Updraft existed at

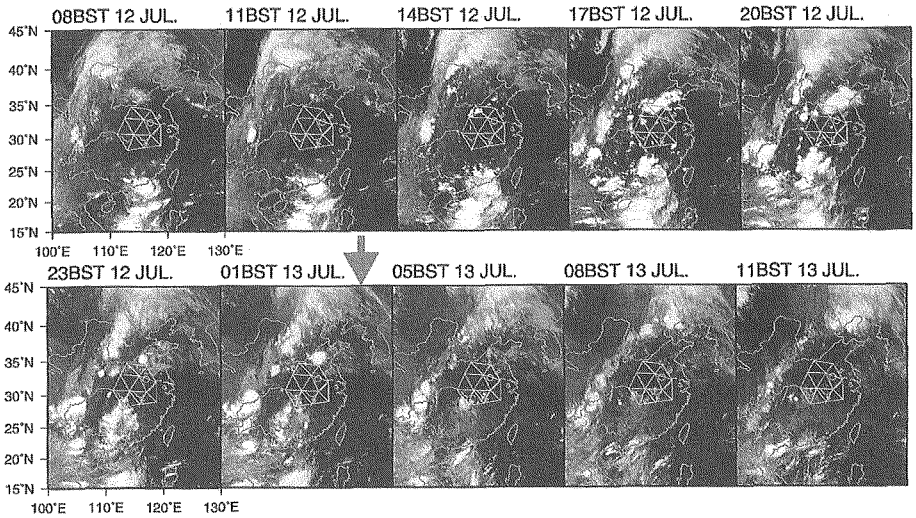

Fig. 19. Three hourly GMS/IR images except 01 BST 13 July from 08 BST 12 July to 11 BST 13 July 1998. The lines and circles represent the sounding sites and radar observation ranges in Fig. 1.

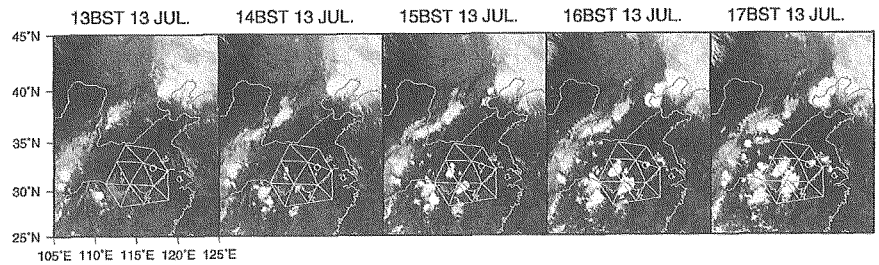

Fig. 20. Hourly GMS/IR images from 13 BST 13 to 17 BST 13 July 1998.

least lower layer in the area around the clusters (A_1, A_2 and A_9 in Fig. 1), and the apparent moisture sink was seen at almost all levels. On the other hand in the area windward of the clusters (A_4, A_5, A_6 and A_7 in Fig. 1), downdraft and apparent moisture source was calculated at all levels. Furthermore the increase of the water vapor was seen in the source area at all levels, while it was limited from 900 hPa to 600 hPa at 20 BST on 12 July (not shown). These results suggests that in the cloud area apparent moisture sink was caused mainly by the condensation while in the windward area apparent moisture source was caused mainly by the evaporation and resulted in the water vapor increase at all levels around the radar site from the night on 12 July to early morning on 13

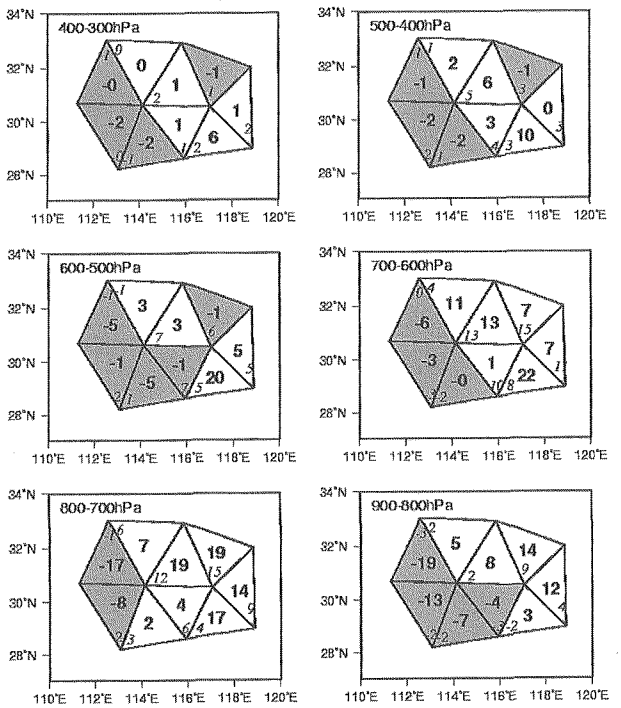

Fig. 21. Apparent moisture sink in AREA2 in Fig. 1 at each level. The bold value at the center of each area shows apparent moisture sink [kg • m^{-2} • day^{-1}] (negative value meaning moisture sink with shading and positive source) and the thin value at the corner shows the increase of water vapor [kg • m^{-2} • day^{-1}].

July.

4. Discussion

4.1 Relationship between environmental condition and convective cloud system

Convectively unstable layer was observed from 10 July to 15 July, and the water vapor especially above 700 hPa increased from 02 BST to 08 BST on 13 July in the vicinity of the radar site followed by the intensification of convective activity in the afternoon of 13 July. It was considered that convective cloud was generated under the convectively unstable condition every day, with the echo top height depending on the amount of water vapor in the middle or upper layer.

A schematic diagram of the structure of convective systems on 11, 13 and 14 July in relation to the environmental wind relative to echo movement was shown

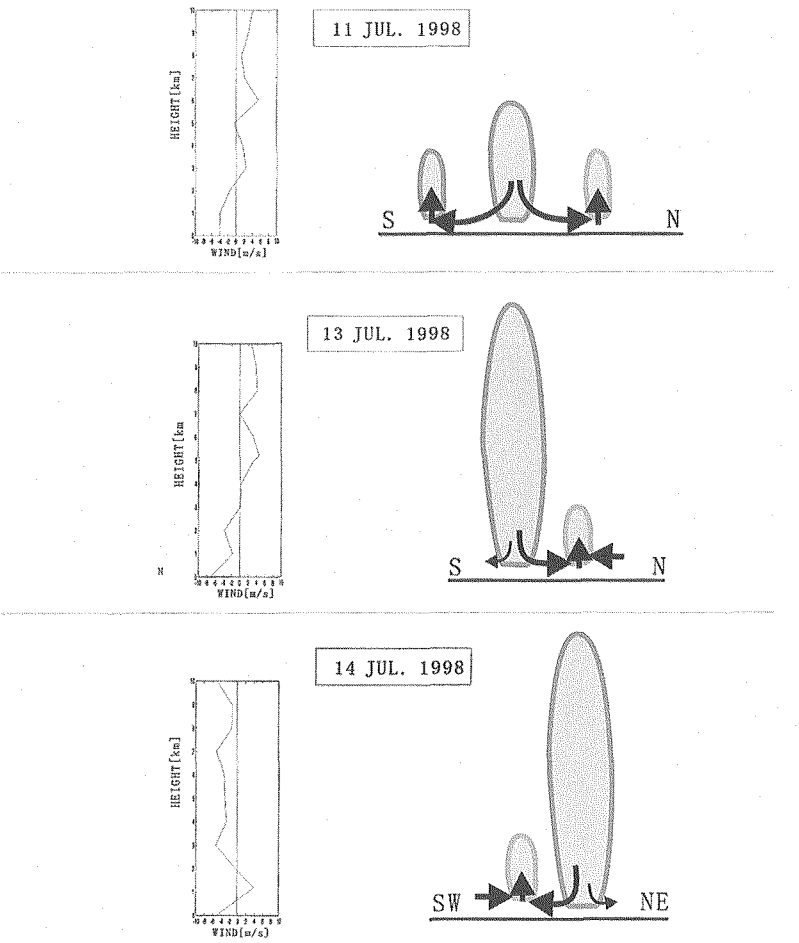

Fig. 22. Schematic diagrams of the structure of the convective cloud systems observed by Huainan Doppler radar on 11, 13, and 14 July 1998.

in Fig. 22. The following explanations are considered for the movement of new echoes. On 11 July, as the environmental vertical wind shear of the horizontal wind was weak below 5 km, which is the typical echo top height, the outflow from downdraft spread in all directions, resulting in producing of new echoes in all sides of the downdraft.

On 13 July, since the environmental wind had strong vertical shear from north to south relative to echo movement, the downdraft had a greater northward speed influenced by southerly wind relative to echo movement in the

middle or upper layer. Therefore the new echo tended to form on the north side of the convection by convergence between the northward outflow and environmental southward wind relative to echo movement.

On 14 July, the strong southwesterly wind in the lower layer made strong vertical shear from southwest to northeast relative to echo movement. Hence, the downdraft tended to form southwestward outflow on the ground causing convergence, also new echoes, on the southwest side of the downdraft.

4.2 Moisture transport

As presented in section 3.3, the cloud clusters associated with tropical cyclone moved to the north with new clouds which were successively generated to the north side during afternoon and at early night. Besides, at late night and during early morning, evaporation from the daytime cloud clusters caused water vapor increase at the windward area at all levels. This seems to make the situation suitable for deep convection during afternoon and at early night on the next day. It is assumed that the cloud clusters associated with tropical cyclone was supplied with much water vapor by sea, and that the water vapor was transported to just south of the front by both the cloud movement in daytime and the evaporation at the windward area at night. When we take the situation into account that the Meiyu front was formed after that, the convective cloud clusters seemed to play an important role in transporting water vapor in the process of formation of the Meiyu front in this case.

5. Conclusions

Radar observations were made during GAME/HUBEX IOP in 1998 from June to July. We analyzed development process of convective cloud systems that located south of the Meiyu front from 10 to 16 July. The features and structures of the convective cloud systems observed in the radar site changed accompanying the increase of water vapor and modification of vertical wind shear as shown in Fig. 23. Diurnal variation of convective rainfall in the afternoon was observed from 10 to 15 July.

On 11 July, because the site was under the subtropical high, the amount of water vapor was small and the vertical wind shear of the horizontal wind below 5 km height was weak. Therefore echo top height was low and outflow from downdraft spread in all directions, resulting in production of new echo cells isotropically. On 13 July, as a cold front approached to radar site, water vapor at middle and upper level increased and the strong southerly wind along the

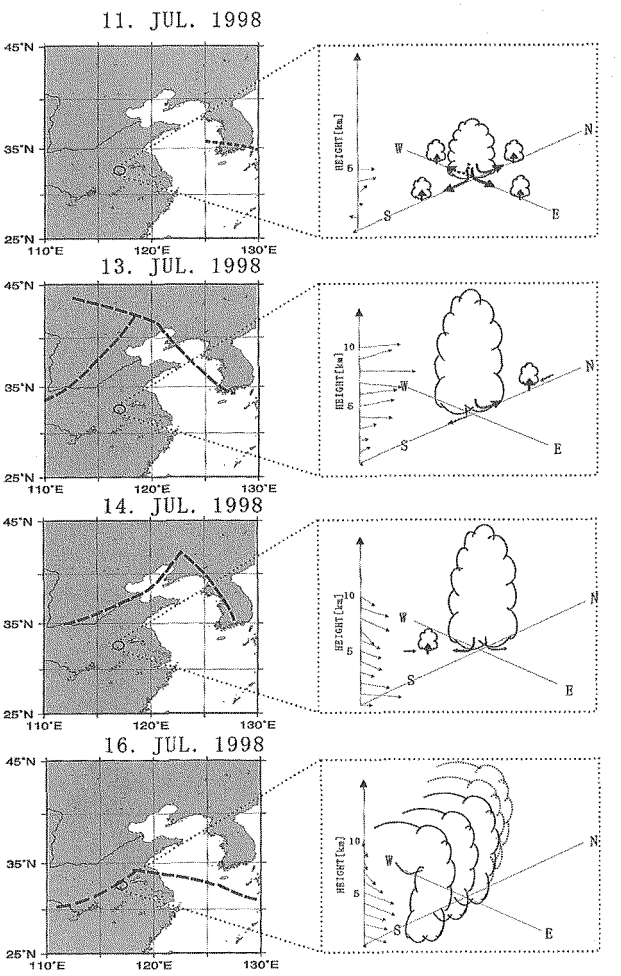

Fig. 23. Schematic diagrams of development process of convective cloud systems relative to the approach of the Meiyu front.

front was observed at the middle and upper level, leading to strong vertical wind shear. For the reason, echo top height turned high and the new echo tended to occur on the north side by convergence between the northward outflow and environmental southward wind relative to echo movement. On 14 July, as the front moved south further, strong southwesterly wind flowing into the Meiyu front was seen. Hence, the downdraft tended to flow southwestward on the ground, causing new echo generation on the southwest side of the downdraft. On 16 July, a squall line was observed just on the Meiyu front in the radar site.

The environmental condition was that strong vertical wind shear parallel to the system movement existed from surface to 4 km height.

Four of these cases can be integrated as follows. The echo top height was influenced by the water vapor in the middle or upper layer while the direction of new echo generation depended on vertical wind shear. Strong advection with the southerly component along and toward the Meiyu front was significant to determine the features of the convective cloud systems in the southern region of the Meiyu front.

Furthermore, it is considered that the water vapor increased around the radar site from the night on 12 July to early morning on 13 July caused by the following two processes. First the cloud clusters associated with tropical cyclone moved to the south of radar site with successive new clouds generation to the north side during afternoon and at night 12 July, second it evaporated around the radar site which located windward side of the cloud at night and during early morning.

We also suggest that two processes are playing important roles in transporting water vapor to the Meiyu front: cluster movement during afternoon and at early night and evaporation at late night and during early morning.

Acknowledgment

The authors express their thanks to the HUBEX Project Office at for providing the sounding data during the period of the GAME/HUBEX IOP. Thanks are also extended to all members of the GAME/HUBEX project for their help in the observations. Thanks are extended to Emeritus Prof. K. Kikuchi, Hokkaido University for his encouragement through this study. The authors wish to express their gratitude to Mr. T. Maesaka, Hokkaido University, for providing useful analyzing tools and valuable comments. This work is partly supported by Grant-in-Aid for Scientific Research of the Ministry of Education, Science, Culture and Sports of Japan.

References

Akiyama, T., 1973a: A geostrophic low-level jet stream in the Baiu season associated with heavy rainfalls over the sea area. J. Meteor. Soc. Japan, **51**, 205-208.

Akiyama, T., 1973b: The large-scale aspects of the characteristic features of the Baiu Front. Pap. Meteorol. Geophys., **24**, 157-188.

Akiyama, T., 1975: Southerly transversal moisture flux into the extremely heavy rainfall zone in the Baiu season. J. Meteor. Soc. Japan, **53**, 304-316.

Barnes, G.M. and K. Sieckman, 1984: The environment fast- and slow-moving tropical mesoscale convective cloud lines. Mon. Wea. Rev., **112**, 1782-1794.

Chen, S-J., Y-H. Kuo, W. Wang, Z-Y. Tao, and B. Cui, 1998: A modeling case study of heavy rainstorms along the Mei-Yu Front. Mon. Wea. Rev., **126**, 2330-2351.

Cressman, G.P., 1959: An operational objective analysis system. Mon. Wea. Rev., **87**, 367-374.

Gal-Chen, T., 1982: Errors in fixed and moving frame of reference: Applications for conventional and Doppler radar analysis. J. Atmos. Sci., **39**, 2279-2300.

Kato, K., J. Matsumoto and H. Iwasaki, 1995: Diurnal variation of Cb-clusters over China and its relation to large-scale conditions in the summer of 1979. J. Meteor. Soc. Japan, **73**, 1219-1234.

Matsumoto, S., S. Yoshizumi and M. Takeuchi, 1970: On the structure of the "Baiu Front" and the associated intermediate scale disturbances in the lower atmosphere. J. Meteor. Soc. Japan, **48**, 479-491.

Matsumoto, S., and K. Ninomiya, 1971: On the mesoscale and medium-scale structure of a cold front and the relevant vertical circulation. J. Meteor. Soc. Japan, **49**, 648-662.

Murakami T., 1959: The general circulation and water-vapor balance over the Far East during the rainy season. Geophys. Mag., **29**, 131-171.

Nakai, S. and R. Kawamura, 1998: Characteristics of cloud clusters appeared around the Baiu Front: Prevailing scale of organized convection and environmental condition. Tenki, **45**, 895-905. (in Japanese)

Ninomiya, K. and T. Akiyama, 1992: Multi-scale features of Baiu, the summer monsoon over Japan and the East Asia. J. Meteor. Soc. Japan, **70**, 467-495.

Saito, N., 1966: A preliminary study of the summer monsoon of Southern and Eastern Asia. J. Meteor. Soc. Japan, **44**, 49-59.

Yanai, M., S. Esbensen, and J-H. Chu, 1973: Determination of bulk properties of tropical cloud clusters from large-scale heat and moisture budget. J. Atmos. Sci., **30**, 611-627.

Zhao, B. and T. Takeda, 1998: Huaihe River Basin Experiment (GAME/HUBEX). Beijing University, 24 pp.